LM-07K004
February 6, 2007

Hafnium Resonance Parameter Analysis Using Neutron Capture and Transmission Experiments

MJ Trbovich, DP Barry, RE Slovacek, Y Danon, RC Block, NC Francis, M Lubert, JA Burke, NJ Drindak, G Lienweber, R Ballad

Hafnium Resonance Parameter Analysis Using Neutron Capture and Transmission Experiments

M. J. Trbovich[1], D. P. Barry[1], R.E. Slovacek, Y. Danon,
R. C. Block, N. C. Francis, M Lubert
Rensselaer Polytechnic Institute, Mechanical, Aerospace and Nuclear Engineering Department
Troy, New York 12180-3590

and

J. A. Burke, N. J. Drindak, G. Leinweber, R. Ballad
Lockheed Martin Company, P.O. Box 1072, Schenectady, New York 12301-1072

Abstract

The focus of this work is to determine the resonance parameters for stable hafnium isotopes in the 0.005 – 200 eV region, with special emphasis on the overlapping ^{176}Hf and ^{178}Hf resonances near 8 eV. Accurate hafnium cross sections and resonance parameters are needed in order to quantify the effects of hafnium found in zirconium, a metal commonly used in reactors. The accuracy of the cross sections and the corresponding resonance parameters used in current nuclear analysis tools are rapidly becoming the limiting factor in reducing the overall uncertainty on reactor physics calculations.

Experiments measuring neutron capture and transmission are routinely performed at the Rensselaer Polytechnic Institute (RPI) LINAC using the time-of-flight technique. ^{6}Li glass scintillation detectors were used for transmission experiments at flight path lengths of 15 and 25 m, respectively. Capture experiments were performed using a sixteen section NaI multiplicity detector at a flight path length of 25 m. These experiments utilized several thicknesses of metallic and isotope-enriched liquid Hf samples. The liquid Hf samples were designed to provide information on the ^{176}Hf and ^{178}Hf contributions to the 8 eV doublet without saturation.

Data analyses were performed using the R-matrix Bayesian code SAMMY. A combined capture and transmission data analysis yielded resonance parameters for all hafnium isotopes from 0.005 – 200 eV. Additionally, resonance integrals were calculated, along with errors for each hafnium isotope, using the NJOY and INTER codes. The isotopic resonance integrals calculated were significantly different than previous values. The ^{176}Hf resonance integral, based on this work, is approximately 73% higher than the ENDF/B-VI value. This is due primarily to the changes to resonance parameters in the 8 eV resonance, the

[1] Now at Lockheed Martin Corporation, P.O. Box 1072, Schenectady, New York 12301-1072

neutron width presented in this work is more than twice that of the previous value. The calculated elemental hafnium resonance integral however, changed very little.

1 Introduction

The majority of measurements and analyses of hafnium cross sections in the region below 200 eV were performed prior to 1965. There were a few measurements by Liou et. al.[1] and Moxon et al.[2] made in the mid 1970's. However, most of the ENDF/B-VI resonance parameters for hafnium in this region are based on much older experiments. These older experiments provided lower resolution data and, due to the tight level spacing of hafnium, lead to many missed resonances. An example of this is best shown in the case of the resonance pair near 8 eV.

A very strong resonance (~25 kb) near 8 eV was attributed solely to ^{178}Hf up until 1974, when measurements by Moxon et al.[2] showed the existence of a ^{176}Hf resonance at nearly the same energy. Although this new resonance made no significant impact on the total neutron cross section for natural hafnium, it did affect the way the hafnium interactions would change with exposure to a neutron flux. This is one example of the importance of accurate resonance parameters for analysis of nuclear systems.

The work described in this paper was completed at the RPI LINAC facility and is described more thoroughly in the doctoral thesis[3] found on file at the RPI Library.

2 Experimental Setup

Transmission experiments at the RPI LINAC are performed in two primary configurations, referred to as "thermal" and "epithermal". Thermal transmission experiments are optimized for low energies (0.001-20 eV) and utilize a ~15 m flight path arrangement. This short flight path provides for a higher intensity of neutrons. The detector used at the ~15 m station is a 5.08 cm (2 inch) diameter and 3 mm thick ^{6}Li loaded glass scintillator that is optically coupled to a photomultiplier tube (PMT). A more detailed description of the complete experimental setup at the RPI LINAC can be found in Reference 4. The samples for the thermal transmission experiments are mounted on a sample changer that is located ~12 m from the neutron production target. The neutron production target used for thermal transmission experiments is the Enhanced Thermal Target[5]. This target is designed to provide the low energy neutrons needed for these experiments.

Epithermal transmission experiments are done with a detector at ~ 25 m away from the neutron production target. This detector is a 12.7 cm (5 inch) diameter and 1.27 cm (0.5 inch) thick ^{6}Li loaded glass scintillator that is optically coupled to a PMT. A rotary sample changer is located ~ 14 m away from the neutron production target. The target used to produce neutrons for the epithermal transmission measurements is knows as the Bounce Target[6] and more recently the Bare Bounce Target[7]. These targets are designed for neutron measurements from a few eV up to approximately 1 keV.

Capture experiments at the RPI LINAC are performed using a 16-segment NaI(Tl) multiplicity type detector[8]. This detector is located approximately 25 m from the neutron production target. Samples are inserted into the center of the detector and held in place by hollow aluminum tubes. Eight samples can be mounted on a wheel that translates and rotates in order to change samples. The detector is inside a 15.24 cm (6 inch) thick lead shield with through-holes for the neutron beam and sample insertion and extraction.

3 Hafnium Samples

The majority of resonances in hafnium below 200 eV were measured using various thicknesses of metallic natural hafnium. The metal samples were all of natural isotopic abundance and were in the form of disks with approximately 5.08 cm (2 inch) diameters. The sample thicknesses of the metallic hafnium used are given in Table I along with the experiments they were used. This variation in sample thickness enabled the analysis of wide-ranging cross sections for the many resonances in hafnium below 200 eV.

The metallic samples did not allow for accurate analysis of the pair of resonances near 8 eV. The total cross section due to the 8 eV resonance pair is predicted to be as high as 30,000 barns. This extremely large cross section at 8 eV ensures that this resonance is saturated in all but the two thinnest metallic samples.

Table I: Metallic hafnium sample specifications. Note that 1 mil is equal to 0.001 inches.

Thickness			Experiment(s) Used In			
Nominal (cm)	Nominal (mil) 1 mil = 0.001 in.	N (atoms/barn)	Thermal Transmission	Thermal Capture	Epi-Thermal Transmission	Epi-Thermal Capture
0.00127	0.5	4.621×10^{-5}				X
0.00254	1	9.984×10^{-5}	X			
0.00508	2	2.369×10^{-4}	X	X		X
0.01016	4	4.537×10^{-4}	X	X		

0.0254	10	1.139×10^{-3}	X	X	X	X
0.0508	20	2.303×10^{-3}	X		X	
0.127	50	5.755×10^{-3}	X		X	X
0.254	100	1.154×10^{-2}			X	

Liquid samples were used in experiments specifically designed for analysis of the 8 eV pair of overlapping Hf^{176} and Hf^{178} resonances. The large cross section of this resonance pair (~30,000 barns) required an extremely thin sample for adequate experimental capture and transmission data. Metal foils could not feasibly be fabricated thin enough with adequate quality for these experiments. The liquid samples provide a more uniform thickness than metal and the thickness can be controlled by the hafnium concentration in the solution.

The liquid samples were created using both natural hafnium oxide and hafnium oxides enriched in ^{178}Hf and ^{176}Hf. The isotopic content of the enriched oxides were measured using a mass spectrometer. Table II shows the results of the mass spectrometer analysis of the enriched hafnium samples in terms of isotopic percentages.

Table II: Isotopic abundance of enriched hafnium samples

	^{174}Hf (atom %)	^{176}Hf (atom %)	^{177}Hf (atom %)	^{178}Hf (atom %)	^{179}Hf (atom %)	^{180}Hf (atom %)	Total Mass (amu)
Enr. ^{176}Hf	0.08	56.17	26.96	10.60	2.49	3.71	176.72
Enr. ^{178}Hf	1.50	1.78	4.20	83.37	5.58	3.56	177.97
^{Nat}Hf	0.162*	5.206*	18.606*	27.297*	13.629*	35.100*	178.49

* These isotopic abundance values are from the Chart of the Nuclides.

Dissolving the hafnium into a liquid solution was thought to be a superior alternative to solid oxide samples. The solution provides a uniform distribution of hafnium as long as the solution is not near its saturation point. The solvent also has to have a low and constant cross section. It was determined that hafnium could be dissolved into deuterated nitric acid (DNO_3). The DNO_3 provided a low, flat cross section in the energy range of interest for these experiments.

Liquid sample hafnium concentrations were based on hafnium densities which would produce transmission values sufficiently above background and below saturation levels to allow for accurate measurements. The first set of liquid samples was called “generation I”. Table III shows the properties of this generation I set of liquid samples, indexed by a unique serial number on each cell. The generation I samples were contained in cells made from two ~ 5.08 cm

(2 in.) diameter quartz flats with a PVC spacer ring glued between them with acid resistant epoxy.

The concentration for each generation I liquid sample is shown in Table III. The concentration of each solution was measured by inductively coupled plasma emission spectroscopy (ICP).

Table III: Generation I liquid samples

Cell #	Type of Hf dissolved	Nominal Liquid Thickness (inches)	Measured Hf Concentration (mg/cm^3)	Hf Number Density (atoms/barn)
Hf-1-1	Enr. ^{176}Hf	0.09375	44.70 ± 0.408	3.888×10^{-5}
Hf-1-2	$D_2O + DNO_3$ Blank	0.09375	-	-
Hf-1-4	Enr. ^{178}Hf	0.09375	24.34 ± 0.062	2.017×10^{-5}
Hf-1-5	Enr. ^{178}Hf	0.09375	12.14 ± 0.072	1.048×10^{-5}
Hf-1-6	Enr. ^{178}Hf	0.09375	3.07 ± 0.021	2.467×10^{-6}
Hf-1-7	Natural	0.09375	35.50 ± 0.146	2.923×10^{-5}

After the experiments with the generation I liquid cells, two of the cells were found to have leaks. The leaks were not significant enough to affect the experimental results; however this prompted a new cell design for the next set of experiments. The new cell design replaced the PVC spacer ring with a quartz ring that was fused in place. This design eliminated the glue joint in the previous generation, which seemed to be the source of leaks. The new cells were referred to as “generation II” cells and were of the same nominal dimensions as the generation I cells. The properties of the generation II liquid samples are given in Table IV.

Table IV: Generation II liquid samples

Cell #	Type of Hf Dissolved	Nominal Liquid Thickness (inches)	Measured Hf Concentration (mg/cm^3)	Hf Number Density (atoms/barn)
Hf-2-2	$D_2O + DNO_3$ Blank	0.09375	-	-
Hf-2-3	Enr. ^{176}Hf	0.09375	26.6 ± 0.5	2.183×10^{-5}

Hf-2-4	Enr. ^{176}Hf	0.09375	9.07 ± 0.18	6.949 x 10^{-6}
Hf-2-5	Enr. ^{176}Hf	0.09375	4.15 ± 0.08	3.639 x 10^{-6}
Hf-2-6	Enr. ^{178}Hf	0.09375	1.63 ± 0.08	1.367 x 10^{-6}
Hf-2-7	Enr. ^{178}Hf	0.09375	0.89 ± 0.045	6.868 x 10^{-7}

4 Data Analysis

The first hafnium data set analyzed was the epithermal metallic transmission data. The ENDF/B-VI resonance parameters were used as starting parameters for the SAMMY[9] fit to the data. A combined fit was performed on the 0.0254 cm (10 mil), 0.0508 cm (20 mil), 0.127 cm (50 mil) and 0.254 cm (100 mil) metallic sample data. This was done by fitting each data set sequentially and using the SAMMY parameter file along with the SAMMY covariance matrix file created by the previous fit as input to the next. After a fit to the transmission data sets with a minimum χ_r^2 (reduced chi-squared[3]) was achieved, epithermal metallic capture data sets were added to the combined analysis. The 0.00127 cm (0.5 mil), 0.00508 cm (2 mil), 0.0254 cm (10 mil), and 0.127 cm (50 mil) sample capture data were added to the fitting sequence of epithermal transmission data sets to form a combined fit. This combined fit sequence was run until a minimum χ_r^2 was achieved.

Not all of the resonance parameters were allowed to vary during the SAMMY fit. If a radiation width parameter, Γ_γ, did not affect the overall fit and was allowed to vary, it was found that the value of this Γ_γ parameter could 'run away'. By this it is meant the radiation width value would continuously increase or decrease with each run of SAMMY without converging. In such cases, the Γ_γ parameter was fixed to an average value of the radiation widths for that particular isotope. This was done based on the assumption that Γ_γ does not vary significantly within an isotope. This average value of Γ_γ was found by averaging the "sensitive" Γ_γ values that were fit by SAMMY within each isotope. Barry[10,11] developed the criteria used to determine which Γ_γ values should be varied. The method was based on the ratio of the radiation width to the neutron width, Γ_γ/Γ_n, and was used to give a sensitivity factor for Γ_γ. The cases where the ratio was less than or approximately equal to 5 gave good indication the fit would be sensitive to Γ_γ. This solved the problem for most of the insensitive Γ_γ values that were running away. However, there were still a few Γ_γ values that were deemed sensitive based on the Barry[10,11] criteria that did not converge. These cases were found in resonances that overlapped a neighboring resonance (or several resonances). In some of these cases, one Γ_γ would constantly change while being compensated for by a nearby resonance's Γ_γ changing in the opposite direction. Through trial and error SAMMY runs, these parameters were also fixed

to an average value of Γ_γ based on the Γ_γ values that did converge for that particular isotope.

The average Γ_γ for each isotope was calculated from a weighted average of the converged Γ_γ values for that isotope. All of the insensitive Γ_γ values were fixed to this average value for that isotope and the fit was repeated in an iterative fashion. This iteration continued until the calculated average Γ_γ for each isotope agreed with the previous iteration's average Γ_γ.

When no further improvements in the fit were apparent and the resonance parameters remained unchanged relative to the previous iteration, the parameters were deemed final. SAMMY was then used to calculate transmission and capture curves based on these final resonance parameters to compare with the experimental data from each sample.

After the resonance parameters were determined for the epithermal region (10 – 200 eV) the thermal data were then analyzed using SAMMY. The thermal transmission data set was analyzed first, and the capture data were added to the analysis once reasonable transmission fits were achieved. The combined analysis of the 0.00254 cm (1 mil), 0.00508 cm (2 mil), 0.01016 cm (4 mil), 0.0254 cm (10 mil), 0.0508 cm (20 mil) and 0.127 cm (50 mil) thermal transmission samples and the 0.00508 cm (2 mil), 0.01016 cm (4 mil) and 0.0254 cm (10 mil) thermal capture samples were run in SAMMY until a minimum χ_r^2 was achieved and there were no significant changes in parameters between runs.

The insensitivity of the low energy resonances to the energy resolution and the Doppler broadening effect allows accurate simultaneous determination of all resonance parameters below 10 eV.

The resonance doublet at 8 eV was not analyzed using the metallic sample data, as it was saturated or close to saturation and provided little information. The thinner isotope-enriched liquid sample data were used to determine the parameters for these resonances.

A sample of the transmission and capture fitted curves and data for a low energy resonance is shown in Figure 1. The 0.0254 cm (10 mil) metallic capture sample shown in Figure 1 shows the effect of a strong resonance with approximately equal scattering and capture probabilities in a relatively thick sample. This effect produces a depression at the resonance energy that is due to the high scattering cross section at the resonance energy, which scatters a large portion of neutrons away from the sample before penetrating the surface. Neutrons which have energies slightly above or below the resonance energy have a much higher probability of penetrating the sample, but will most likely interact inside the sample. The neutrons that scatter once inside the sample will most likely be captured before leaving the sample, creating increased counts in the wings of the resonance. Table VII contains the final resonance parameters determined from this analysis, on which all of these fits are based.

The resonance parameters for the ^{176}Hf and ^{178}Hf resonances near 8 eV were determined from the isotope enriched liquid sample data. Two generations of these samples were run in both capture and transmission experiments, as described previously. The transmission experiment data using the generation I

and II liquid samples were analyzed first using SAMMY. Once the transmission data were fitted, the capture data were added to the analysis. The combined transmission and capture analysis showed significant differences between the data sets. The yield values from the capture data did not agree with the transmission data over the energy range being analyzed. Because of this, SAMMY was initially unable to determine a set of parameters that fit all of these data sets.

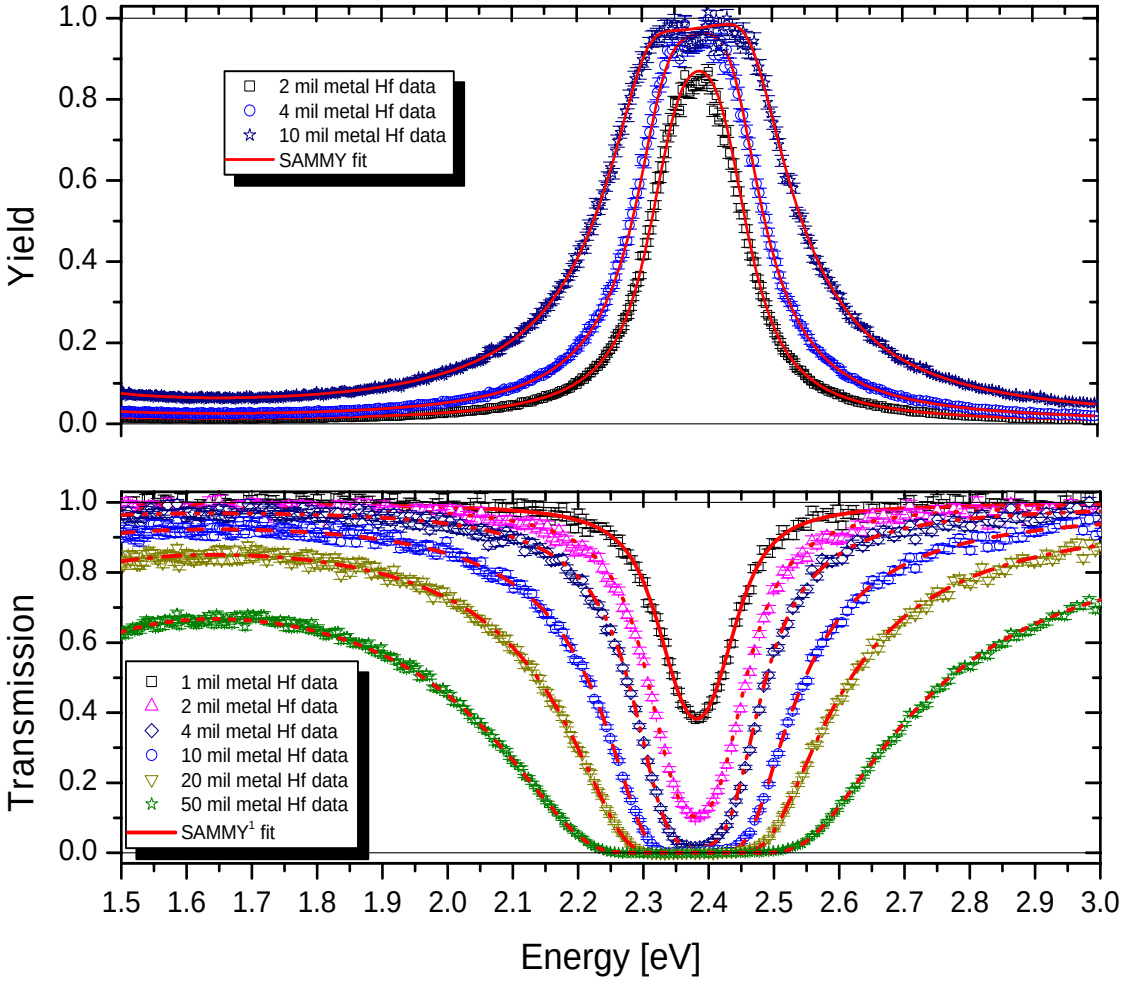

Figure 1: Thermal metallic hafnium transmission and capture data with SAMMY calculated transmission from fitted resonance parameters

In order to determine if there was a problem with the flux normalization of the capture data or if there was a difference in detection efficiency between isotopes, the 8 eV resonance parameters fitted to the transmission data were used to calculate the expected yield for the capture experiments using SAMMY. The energy region being analyzed was increased to include surrounding ^{177}Hf resonances. The parameters for these resonances had been determined from the previously described analyses using natural metallic samples. The yield

curve, calculated from the transmission data, was then applied to the capture data for comparison; Figure 2 shows this comparison for a ^{176}Hf enriched liquid sample. Figure 2 shows that the region over the 8 eV doublet is the only area of significant disagreement. The surrounding ^{177}Hf resonances in Figure 2 show good agreement between the yield data and the calculated yield from the transmission fitted resonance parameters. The lower yield data over the 8 eV doublet was an indication of a lower detection efficiency for ^{176}Hf and ^{178}Hf neutron capture gamma rays relative to those from neutron capture in ^{177}Hf, which was used for flux normalization (at the 1.1 eV resonance).

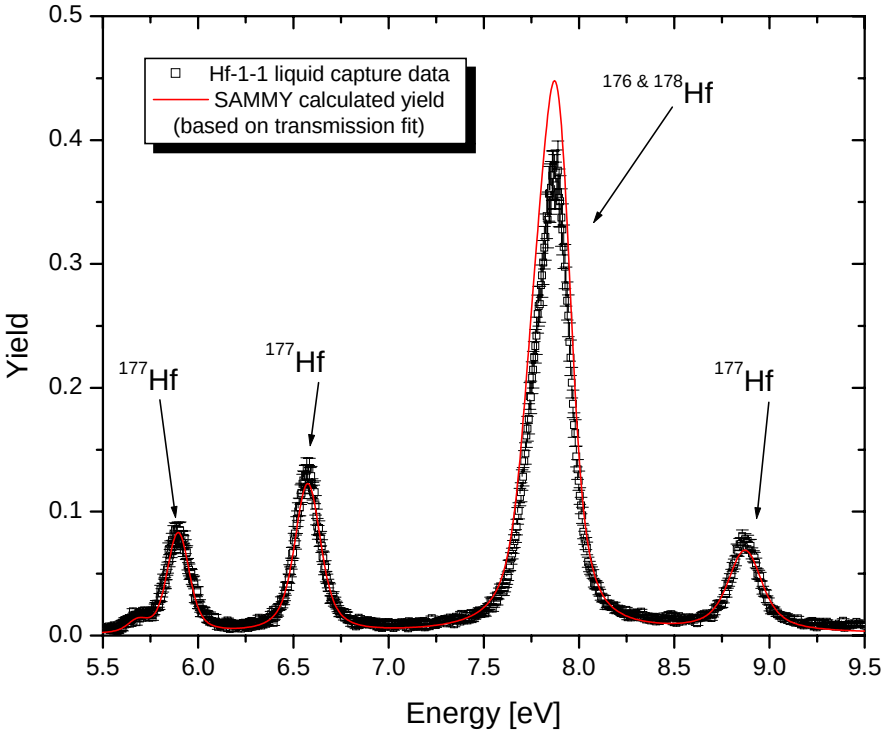

Figure 2: ^{176}Hf enriched liquid capture data compared to calculated yield based on 8 eV resonance parameters fitted to transmission data showing the normalization problem

The multiplicity distribution for these isotopes was examined to look for significant differences in average multiplicity. Differences in average multiplicity could indicate differences in detection efficiency, due to differences in the number of gamma rays emitted or in the energy of the gamma rays. Figure 3 shows a plot of the fraction of total counts versus multiplicity number. The counts for each unit of multiplicity were summed over a resonance for each of the isotopes ^{176}Hf, ^{177}Hf and ^{178}Hf. The 8 eV resonance in the ^{178}Hf enriched liquid sample data was used to obtain the multiplicity distribution for ^{178}Hf, and the 48 eV resonance in the ^{176}Hf enriched liquid sample data was used for ^{176}Hf. The 1 eV resonance was used to get the ^{177}Hf multiplicity distribution. This plot shows that ^{177}Hf has a higher average multiplicity (4.2) than ^{176}Hf and ^{178}Hf (3.8). This means that on average a neutron capture in ^{177}Hf produces approximately 11%

more gamma rays than a neutron capture in ^{176}Hf or ^{178}Hf. This higher number of capture gamma rays should increase the chance for detecting a capture event in ^{177}Hf relative to ^{176}Hf or ^{178}Hf.

The binding energy for each isotope can also have an effect on detection efficiency by determining the total energy emitted by the capture gamma rays. Table VII shows the binding energy for ^{176}Hf, ^{177}Hf and ^{178}Hf along with the average multiplicity at selected resonances. The higher binding energy of ^{177}Hf, along with the higher average multiplicity, are expected to increase the probability of detection due to more energy and gamma rays being released on average for each capture event. This effect would cause the detection efficiency for ^{177}Hf to be relatively larger and thus a lower yield would be observed for ^{176}Hf and ^{178}Hf resonances relative to ^{177}Hf resonances. This trend is also in agreement with detection efficiency calculations based on capture gamma ray cascades in hafnium done using the code DICEBOX[12].

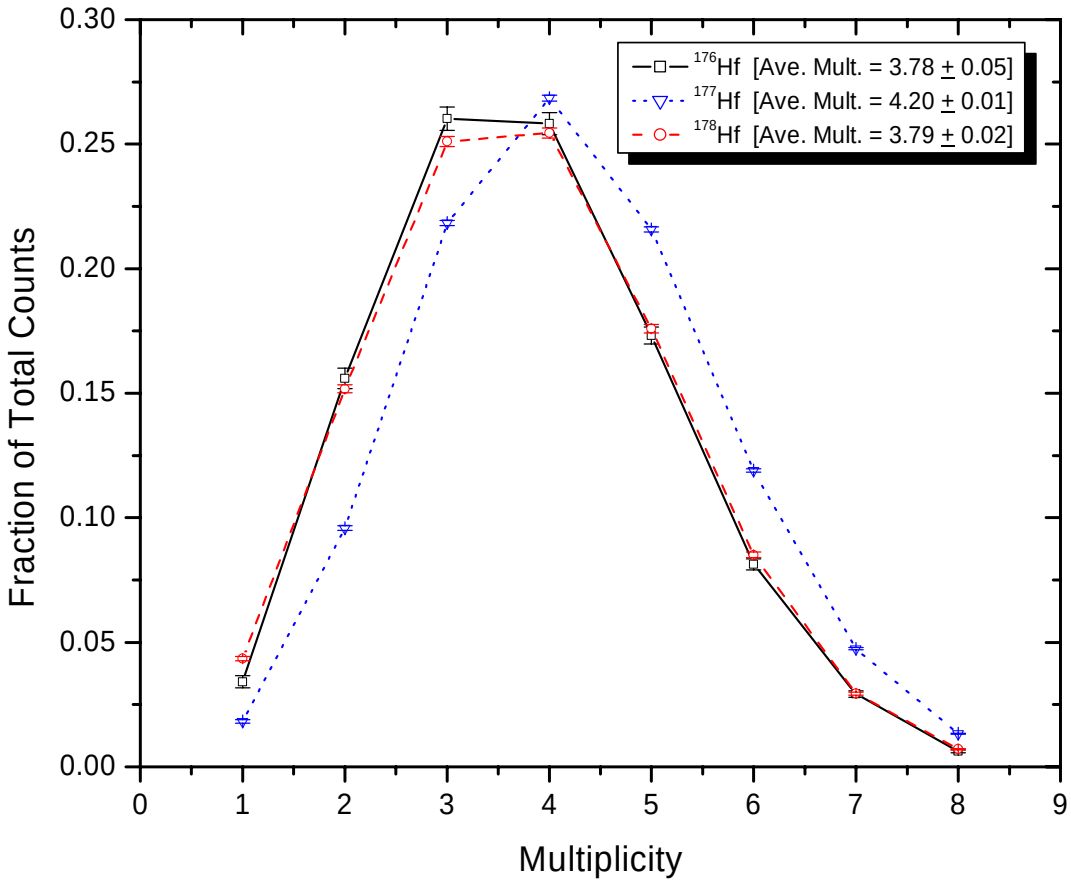

Figure 3: Multiplicity distribution for ^{176}Hf, ^{177}Hf and ^{178}Hf

Table VII: Binding energy[13] and average multiplicity for ^{176}Hf, ^{177}Hf and ^{178}Hf

Isotope	Binding Energy (MeV)	Average Multiplicity
^{176}Hf	6.3833 ± 0.002	3.78 ± 0.05
^{177}Hf	7.6263 ± 0.0009	4.20 ± 0.01
^{178}Hf	6.0998 ± 0.0008	3.79 ± 0.02

SAMMY was used to fit a normalization factor that would correct for the difference in detection efficiency. This was accomplished by using the resonance parameters fitted to the liquid transmission data as input to SAMMY. A combined fit of all capture data sets was then run allowing only normalization to vary. This analysis determined there was 24% difference between the yield data and the SAMMY calculated yield from the transmission fitted parameters. The ^{176}Hf and ^{178}Hf detection efficiencies were comparable due to their similar average multiplicity and binding energy. This normalization factor was then used to correct the yield data.

A combined transmission and capture data analysis was then performed using the corrected capture data. This analysis included both first and second generation liquid sample data from capture and transmission experiments. Figure 4 shows a plot of ^{176}Hf enriched liquid sample capture data with calculated curves based on both ENDF/B-VI.1 resonance parameters and those determined from this analysis. The fit to the ^{176}Hf enriched samples is not as good as that to the ^{178}Hf enriched samples. Figure 4 shows the fit slightly under predicting the transmission of the thickest sample (Hf-1-1) and over predicting the two thinner samples (Hf-2-4 and Hf-2-5). These inconsistencies may be due to inaccuracies in the solution contents of the ^{176}Hf enriched liquid samples. The fits for these samples are still acceptable, and are a significant improvement over the yields calculated from the ENDF/B-VI.1 values, as shown in Figure 4. Figure 5 shows the transmission results for the ^{176}Hf enriched samples, which show good agreement between experiment and calculated values. Figure 6 shows the capture results for ^{178}Hf enriched samples compared to ENDF/B-VI.1 values. Figure 6 also shows significantly better agreement between experiment and calculated yields for the ^{178}Hf parameters derived in this analysis as compared to those based on ENDF/B-VI.1 parameters. Figure 7 shows the transmission results for the ^{178}Hf enriched samples, which also show good agreement between experiment and calculated transmission values, based on resonance parameters determined in this analysis.

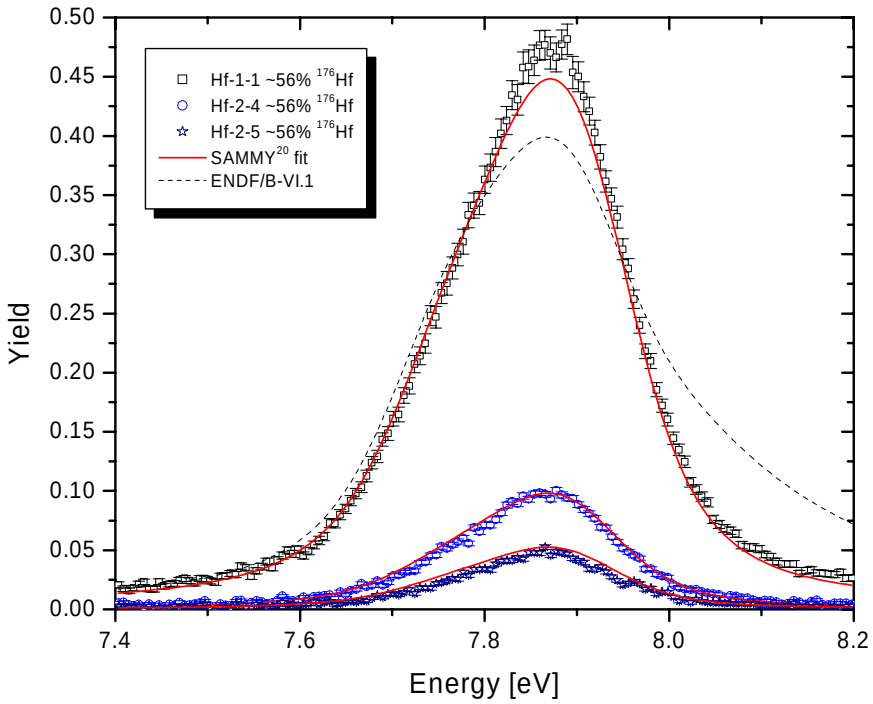

Figure 4: ^{176}Hf enriched liquid capture samples with SAMMY calculated yield from fitted resonance parameters and calculated yield based on ENDF/B-VI.1 parameters

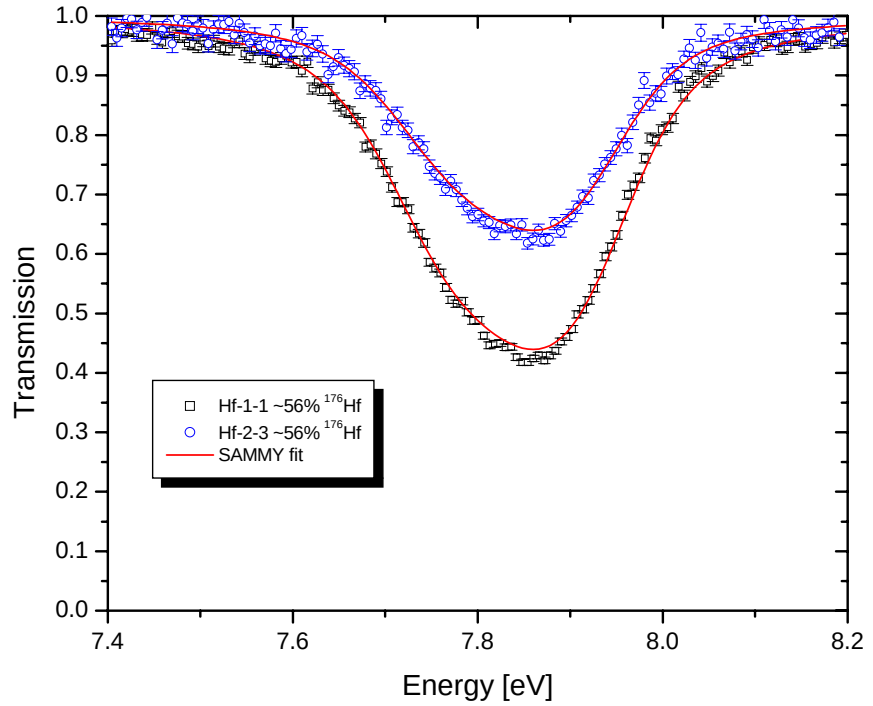

Figure 5: ^{176}Hf enriched liquid transmission samples with SAMMY calculated transmission from fitted resonance parameters

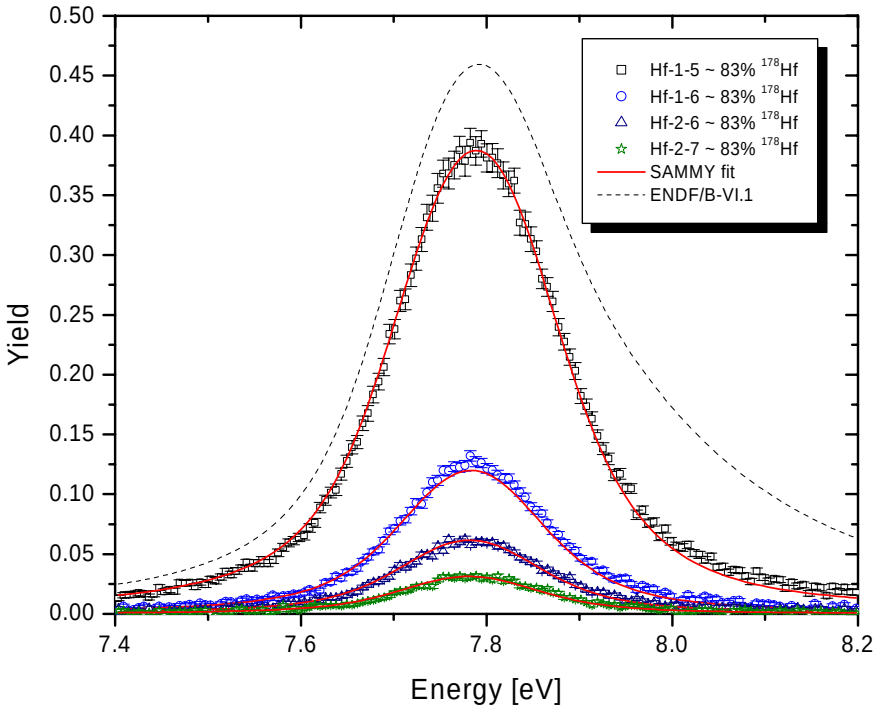

Figure 6: ^{178}Hf enriched liquid capture samples with SAMMY calculated yield from fitted resonance parameters and calculated yield based on ENDF/B-VI.1 parameters

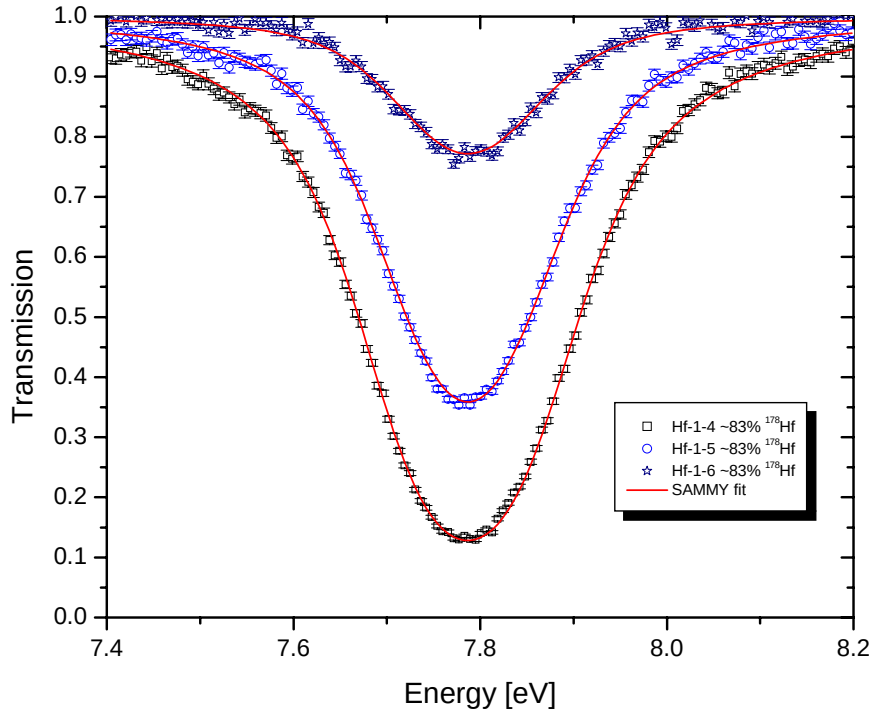

Figure 7: ^{178}Hf enriched liquid transmission samples with SAMMY calculated transmission from fitted resonance parameters

5 Results

Resonance parameters determined from the previously described analyses are presented in Table VIII, shown as the RPI resonance parameters. Two error values are reported for the RPI resonance parameters. The error value determined by SAMMY is shown in parenthesis and is based primarily on the statistical accuracy of the experimental data used in the fit. The error value shown in square brackets is an estimate of the error in the resonance parameters due to uncertainties in the resolution function. Reference 3 contains a detailed description of the methods used to calculate the uncertainties shown in Table VIII

Table VIII also shows the ENDF/B-VI parameters, which were used as starting values for the SAMMY analysis, and the parameters reported from Moxon et al.[2] The Γ_γ values with errors in curly brackets { } are those resonances that were deemed insensitive to changes in Γ_γ and were set to the average Γ_γ value for that isotope. The error quoted for these average values of Γ_γ is one standard deviation.

Table VIII: Fitted RPI resonance parameters compared to ENDF/B-VI and those measured by Moxon[2]

RPI statistical errors given as one standard deviation as calculated by SAMMY are in ( ).
Errors propagated from resolution function uncertainties are in [ ].
The standard deviation of the isotope average Γ_γ is shown in { }, only where the average Γ_γ was used.
Errors from Moxon[2], one standard deviation, are in ||.

Energy [eV]			**Γ_γ [meV]**			**Γ_n [meV]**			**Isotope & Spin**
RPI	ENDF B-VI	Moxon[2]	RPI	ENDF B-VI	Moxon[2]	RPI	ENDF B-VI	Moxon[2]	
^{174}Hf									
4.06 (0.04)	4.25	-	52 (5) [0.002]	60	-	0.015 (0.001) [0.0000]	0.017	-	174 I = 0 J = ½
13.373 (0.004)	13.38	13.38 |0.003|	65 {29}	60	-	5.7 (0.2) [0.05]	4.8	3.657 |0.75|	174 I = 0 J = ½
29.985 (0.003)	30	-	65 {29}	60	-	36.3 (0.8) [0.1]	40	-	174 I = 0 J = ½
70.66 (0.02)	70.5	-	65 {29}	60	-	24 (2) [2]	12	-	174 I = 0 J = ½
77.85 (0.01)	77.9	-	51 (4) [2]	60	-	83 (4) [1]	65	-	174 I = 0 J = ½
106.95 (0.02)	107.1	-	65 {29}	60	-	177 (10) [10]	122	-	174 I = 0 J = ½

Energy [eV]			Γ_γ [meV]			Γ_n [meV]			Isotope & Spin
RPI	ENDF B-VI	Moxon[2]	RPI	ENDF B-VI	Moxon[2]	RPI	ENDF B-VI	Moxon[2]	
124.36 (0.03)	124.6	-	65. {29}	60	-	680 (27) [15]	50	-	174 I = 0 J = ½
147.63 (0.04)	147.6	-	102 (10) [9]	60	-	358 (24) [22]	120	-	174 I = 0 J = ½
153.40 (0.04)	153.5	-	65 {29}	60	-	219 (17) [10]	85	-	174 I = 0 J = ½
^{176}Hf									
7.8891 (0.0003)	7.886	7.8858 |0.01|	61.8 (0.6) [0.05]	57	57 |12|	10.15 (0.04) [0.009]	4.71	4.71 |5.5|	176 I = 0 J = ½
48.2540 (0.0009)	48.3	-	49 (0.4) [1]	51	-	107 (0.5) [2]	125	-	176 I = 0 J = ½
53.282 (0.004)	53.3	-	55 {9}	51	-	1.69 (0.03) [0.009]	1.9	-	176 I = 0 J = ½
67.218 (0.002)	67.1	-	55 {9}	51	-	26.0 (0.6) [0.0000]	15	-	176 I = 0 J = ½
124.079 (0.008)	123.9	-	55 {9}	51	-	32 (1) [2]	42	-	176 I = 0 J = ½
177.15 (0.01)	177.1	-	55 {9}	51	-	86 (3) [4]	47	-	176 I = 0 J = ½
^{177}Hf									
1.1001 (0.0001)	1.098	1.0964 |0.0015|	65.23 (0.08) [0.009]	66.2	65.64 |2.86|	2.225 (0.002) [0.002]	2.171	2.232 |0.013|	177 I = 7/2 J = 3
2.3868 (0.0001)	2.388	2.3837 |0.0002|	60.7 (0.2) [0.009]	60.8	61.74 |0.74|	8.04 (0.02) [0.006]	8	8.068 |0.068|	177 I = 7/2 J = 4
5.9002 (0.0002)	5.89	5.8937 |0.0009|	62 (0.5) [2]	54.8	65.47 |3.34|	5.32 (0.02) [0.05]	6.743	5.348 |0.127|	177 I = 7/2 J = 3
6.5780 (0.0002)	6.6	6.5691 |0.0014|	55.6 (0.3) [0.8]	65	64.96 |1.76|	8.21 (0.03) [0.06]	8.089	8.049 |0.048|	177 I = 7/2 J = 4
8.8766 (0.0002	8.88	8.8388 |0.0008|	57.3 (0.4) [0.3]	65	64.97 |1.73|	5.89 (0.02) [0.03]	6.044	5.705 |0.088|	177 I = 7/2 J = 4

Energy [eV]			Γ_γ [meV]			Γ_n [meV]			Isotope & Spin
RPI	ENDF B-VI	Moxon[2]	RPI	ENDF B-VI	Moxon[2]	RPI	ENDF B-VI	Moxon[2]	
10.9607 (0.0007)	10.95	10.941 |0.009|	57 {13}	65	75.52 |9.42|	0.490 (0.003) [0.002]	0.56	0.497 |0.013|	177 I = 7/2 J = 3
13.6810 (0.0008)	13.67	13.687 |0.002|	57 {13}	65	64.82 |6.56|	0.603 (0.004) [0.002]	0.702	0.543 |0.031|	177 I = 7/2 J = 4
13.9696 (0.0003)	13.96	13.971 |0.003|	57 {13}	83.7	74.56 |4.79|	2.71 (0.009) [0.01]	3.314	3.064 |0.073|	177 I = 7/2 J = 3
21.9844 (0.0007)	21.97	22.0052 |0.0014|	57 {13}	65	67.34 |5.24|	1.7633 (0.009) [0.009]	1.902	1.565 |0.041|	177 I = 7/2 J = 4
22.298 (0.002)	22.26	22.3117 |0.0061|	57 {13}	65	102.6 |12.2|	0.840 (0.009) [0.002]	0.857	0.759 |0.047|	177 I = 7/2 J = 3
23.426 (0.002)	23.44	23.5205 |0.008|	57 {13}	65	84.6 |10.0|	1.32 (0.02) [0.03]	1.458	1.59 |0.64|	177 I = 7/2 J = 4
25.641 (0.002)	25.64	25.665 |0.001|	57 {13}	65	-	0.545 (0.008) [0.002]	0.502 857	0.473 |0.0037|	177 I = 7/2 J = 3
27.0364 (0.0008)	27.01	27.063 |0.01|	57 {13}	65	88.1 |11.0|	2.84 (0.02) [0.02]	3.085 714	2.78 |0.16|	177 I = 7/2 J = 3
31.608 (0.005)	31.58	-	57 {13}	65	-	0.36 (0.01) [0.009]	0.343	-	177 I = 7/2 J = 3
32.841 (0.001)	32.82	-	57 {13}	65	-	1.30 (0.01) [0.005]	1.404	-	177 I = 7/2 J = 4
36.095 (0.001)	36.08	-	57 {13}	65	-	3.53 (0.03) [0.03]	3.531	-	177 I = 7/2 J = 3
36.9805 (0.0008)	36.95	-	57 {13}	56	-	8.92 (0.05) [0.06]	9.689	-	177 I = 7/2 J = 4
43.082 (0.001)	43.05	-	57 {13}	65	-	5.13 (0.03) [0.03]	5.173 333	-	177 I = 7/2 J = 4
45.165 (0.001)	45.11	-	57 {13}	65	-	3.37 (0.02) [0.02]	3.377 778	-	177 I = 7/2 J = 4
46.256 (0.001)	46.22	-	57 {13}	78	-	7.00 (0.04) [0.07]	6.969	-	177 I = 7/2 J = 4

Energy [eV]			Γ_γ [meV]			Γ_n [meV]			Isotope & Spin
RPI	ENDF B-VI	Moxon[2]	RPI	ENDF B-VI	Moxon[2]	RPI	ENDF B-VI	Moxon[2]	
48.861 (0.001)	48.76	-	57 (1) [5]	82	-	36 (0.3) [1]	33.14	-	177 I = 7/2 J = 3
49.627 (0.001)	49.56	-	57 {13}	65	-	5.92 (0.04) [0.08]	5.244	-	177 I = 7/2 J = 4
54.815 (0.001)	54.71	-	57 {13}	69	-	20.6 (0.1) [0.2]	15.11	-	177 I = 7/2 J = 4
56.402 (0.001)	56.29	-	57 {13}	70	-	14.2 (0.08) [0.1]	14.06	-	177 I = 7/2 J = 3
57.082 (0.002)	57	-	57 {13}	65	-	4.23 (0.04) [0.02]	4.089	-	177 I = 7/2 J = 4
59.323 (0.002)	59.21	-	57 {13}	65	-	4.2535 (0.04) [0.03]	4.217 143	-	177 I = 7/2 J = 3
62.228 (0.004)	62.15	-	57 {13}	65	-	1.63 (0.03) [0.02]	1.509	-	177 I = 7/2 J = 3
63.552 (0.001)	63.42	-	54.3 (0.4) [0.7]	55	-	70.2 (0.3) [0.7]	64.89	-	177 I = 7/2 J = 4
66.773 (0.007)	66.69	-	119* (2)	65	-	41.6* (0.5)	49.14	-	177 I = 7/2 J = 3
70.098 (0.009)	69.96	-	57 {13}	65	-	0.68 (0.03) [0.006]	0.471	-	177 I = 7/2 J = 4
71.440 (0.001)	71.29	-	57 {13}	54	-	14.08 (0.09) [0.1]	14.58	-	177 I = 7/2 J = 4
72.05 (0.02)	72.22	-	72* (7)	65	-	2.2011* (0.03)	1.669	-	177 I = 7/2 J = 3
75.672 (0.007)	75.41	-	57 {13}	65	-	2.9 (0.09) [0.2]	2.057	-	177 I = 7/2 J = 3
76.135 (0.002)	75.99	-	57 {13}	65	-	15.0 (0.1) [0.3]	16.53	-	177 I = 7/2 J = 4
82.35 (0.01)	82.33	-	57 {13}	65	-	0.64 (0.02) [0.02]	0.542	-	177 I = 7/2 J = 4

Energy [eV]			Γ_γ [meV]			Γ_n [meV]			Isotope & Spin
RPI	ENDF B-VI	Moxon[2]	RPI	ENDF B-VI	Moxon[2]	RPI	ENDF B-VI	Moxon[2]	
84.762 (0.002)	84.56	-	57 {13}	75	-	23.5 (0.2) [0.3]	24.36	-	177 I = 7/2 J = 4
85.31 (0.08)	85.25	-	57 {13}	65	-	0.38 (0.05) [0.07]	3.429	-	177 I = 7/2 J = 3
86.861 (0.007)	86.73	-	57 {13}	65	-	1.14 (0.03) [0.02]	0.924	-	177 I = 7/2 J = 4
88.639 (0.003)	88.51	-	57 {13}	65	-	4.58 (0.06) [0.04]	4.571	-	177 I = 7/2 J = 3
93.312 (0.006)	93.13	-	57 {13}	65	-	4.7 (0.1) [0.1]	4.8	-	177 I = 7/2 J = 3
97.208 (0.002)	97.01	-	98 (3) [13]	60	-	17.4 (0.1) [0.3]	19.2	-	177 I = 7/2 J = 4
102.5 (0.1)	98.9	-	57 {13}	65	-	0.019 (0.002) [0.0003]	0.871	-	177 I = 7/2 J = 4
103.258 (0.002)	103.07	-	57 {13}	63	-	59 (0.6) [1]	55.77	-	177 I = 7/2 J = 3
111.56 (0.01)	111.5	-	57 {13}	65	-	2.3 (0.1) [0.02]	2.514	-	177 I = 7/2 J = 3
112.030 (0.007)	111.96	-	57 {13}	65	-	4.1 (0.1) [0.04]	4	-	177 I = 7/2 J = 4
115.243 (0.005)	115	-	57 {13}	65	-	4.05 (0.06) [0.06]	0.231	-	177 I = 7/2 J = 4
121.34 (0.01)	121.2	-	57 {13}	65	-	4.2 (0.2) [0.06]	4.914	-	177 I = 7/2 J = 3
122.1 (0.1)	122.7	-	57 {13}	65	-	2.5 (0.2) [0.1]	5.029	-	177 I = 7/2 J = 3
122.18 (0.02)	122.8	-	57 {13}	65	-	0.54 (0.05) [0.009]	0.709	-	177 I = 7/2 J = 3
123.88 (0.01)	123.7	-	57 {13}	65	-	8 (0.4) [1]	10.29	-	177 I = 7/2 J = 3

Energy [eV]			Γ_γ [meV]			Γ_n [meV]			Isotope & Spin
RPI	ENDF B-VI	Moxon[2]	RPI	ENDF B-VI	Moxon[2]	RPI	ENDF B-VI	Moxon[2]	
126.36 (0.02)	126.2	-	57 {13}	65	-	0.82 (0.03) [0.02]	0.613	-	177 I = 7/2 J = 4
131.843 (0.002)	131.6	-	67 (1) [2]	66	-	59 (0.6) [2]	60.94	-	177 I = 7/2 J = 3
134.245 (0.006)	134	-	57 {13}	65	-	4.21 (0.08) [0.06]	3.733	-	177 I = 7/2 J = 4
136.27 (0.02)	136.2	-	57 {13}	65	-	1.7 (0.07) [0.2]	0.743	-	177 I = 7/2 J = 3
138.061 (0.005)	137.4	-	57 {13}	65	-	16.2 (0.3) [0.6]	12	-	177 I = 7/2 J = 4
141.351 (0.003)	141.1	-	57 {13}	54	-	21.1 (0.2) [0.2]	23.47	-	177 I = 7/2 J = 4
143.16 (0.02)	143.2	-	57 {13}	65	-	3.7 (0.2) [0.2]	4.96	-	177 I = 7/2 J = 3
143.84 (0.01)	143.7	-	57 {13}	65	-	9.5 (0.4) [0.6]	10.49	-	177 I = 7/2 J = 4
145.793 (0.006)	145.5	-	57 {13}	65	-	7.6 (0.1) [0.01]	7.371	-	177 I = 7/2 J = 3
148.765 (0.004)	148.5	-	57 {13}	65	-	21.0 (0.3) [0.5]	21.26	-	177 I = 7/2 J = 3
151.30 (0.03)	151.2	-	57 {13}	65	-	0.67 (0.05) [0.006]	0.409	-	177 I = 7/2 J = 4
152.67 (0.01)	152.9	-	57 {13}	65	-	3.82 (0.09) [0.08]	1.867	-	177 I = 7/2 J = 4
154.88 (0.02)	156.1	-	57 {13}	65	-	1.53 (0.07) [0.06]	3.2	-	177 I = 7/2 J = 3
160.229 (0.008)	160	-	57 {13}	65	-	3.91 (0.08) [0.05]	3.467	-	177 I = 7/2 J = 4
163.284 (0.003)	163	-	57 {13}	60	-	45.8 (0.6) [0.6]	44.57	-	177 I = 7/2 J = 3

Energy [eV]			Γ_γ [meV]			Γ_n [meV]			Isotope & Spin
RPI	ENDF B-VI	Moxon[2]	RPI	ENDF B-VI	Moxon[2]	RPI	ENDF B-VI	Moxon[2]	
167.596 (0.007)	167.3	-	57 {13}	65	-	9.346 (0.2) [0.1]	8.286	-	177 I = 7/2 J = 3
171.06 (0.01)	171	-	57 {13}	65	-	10 (0.2) [1]	12.91	-	177 I = 7/2 J = 3
174.326 (0.007)	174.2	-	57 {13}	65	-	27 (0.9) [3]	12.44	-	177 I = 7/2 J = 4
176.325 (0.008)	176.1	-	57 {13}	65	-	45 (1) [6]	56	-	177 I = 7/2 J = 3
176.88 (0.03)	176.7	-	57 {13}	65	-	9 (1) [0.2]	44.44	-	177 I = 7/2 J = 4
179.31 (0.06)	178.9	-	57 {13}	65	-	0.46 (0.04) [0.008]	0.667	-	177 I = 7/2 J = 4
181.35 (0.01)	181.1	-	57 {13}	65	-	5.6 (0.1) [0.07]	5.156	-	177 I = 7/2 J = 4
184.90 (0.02)	184.5	-	57 {13}	65	-	1.66 (0.07) [0.04]	1.262	-	177 I = 7/2 J = 4
188.48 (.03)	188	-	57 {13}	65	-	1.8 (0.2) [0.02]	0.587	-	177 I = 7/2 J = 4
193.012 (0.006)	192.7	-	57 {13}	65	-	15.0 (0.3) [0.07]	6.933	-	177 I = 7/2 J = 4
194.400 (0.009)	194	-	57 {13}	65	-	9.8 (0.2) [0.1]	8.571	-	177 I = 7/2 J = 3
199.488 (0.006)	199.1	-	57 {13}	72	-	21.0 (0.4) [0.2]	21.16	-	177 I = 7/2 J = 4
^{178}Hf									
7.7865 (0.0001)	7.78	7.7718 |0.0017|	53.0 (0.2) [0.1]	60	57.67 |1.6|	53.83 (0.08) [0.007]	50	52.13 |1.42|	178 I = 0 J = ½
-	-	28.672 |0.01|	-	-	-	-	-	-	178 I = 0 J = ½
104.904 (0.002)	104.8	-	53**	51	-	7.16 (0.05) [0.08]	8.9	-	178 I = 0 J = ½

Energy [eV]			Γ_γ [meV]			Γ_n [meV]			Isotope & Spin
RPI	ENDF B-VI	Moxon[2]	RPI	ENDF B-VI	Moxon[2]	RPI	ENDF B-VI	Moxon[2]	
164.707 (0.003)	164.6	-	53**	51	-	13.5 (0.1) [0.06]	15	-	178 I = 0 J = ½
^{179}Hf									
5.6885 (0.0002)	5.68	5.686 |0.001|	47 (0.4) [2]	62	62.64 |2.96|	4.27 (0.02) [0.04]	4.6	4.64 |0.092|	179 I = 9/2 J = 5
17.6533 (0.0006)	17.65	17.658 |0.0005|	52 {8}	66	64.13 |3.22|	2.09 (0.01) [0.009]	2.333	2.065 |0.031|	179 I = 9/2 J = 4
19.131 (0.004)	19.13	19.1355 |0.0006|	52 {8}	66	-	0.124 (0.004) [0.0004]	0.109	0.107 |0.01|	179 I = 9/2 J = 5
23.6577 (0.0006)	23.7	23.666 |0.008|	52 {8}	66	64.1 |9|	7.47 (0.05) [0.09]	7.546	7.68 |0.73|	179 I = 9/2 J = 5
26.540 (0.002)	26.5	26.535 |0.011|	52 {8}	66	89.3 |10|	1.27 (0.01) [0.005]	1.333	1.14 |0.1|	179 I = 9/2 J = 4
27.418 (0.004)	27.35	27.405 |0.012|	52 {8}	66	63.7 |11|	0.433 (0.009) [0.005]	0.391	0.415 |0.05|	179 I = 9/2 J = 5
31.156 (0.006)	31.14	-	52 {8}	66	-	8.1447 (0.04) [0.06]	8.333	-	179 I = 9/2 J = 4
36.520 (0.007)	36.5	-	52 {8}	66	-	26.00 (0.02) [0.04]	27.27	-	179 I = 9/2 J = 5
40.1350 (0.0005)	40.12	-	61 (0.8) [3]	66	-	23.5 (0.1) [0.4]	22.73	-	179 I = 9/2 J = 5
42.3270 (0.0007)	42.29	-	52 {8}	66	-	15.3 (0.08) [0.2]	14.44	-	179 I = 9/2 J = 4
50.785 (0.005)	50.77	-	52 {8}	66	-	1.11 (0.03) [0.007]	1.455	-	179 I = 9/2 J = 5
51.149 (0.009)	54.79	-	52 {8}	66	-	0.71 (0.03) [0.005]	5.889	-	179 I = 9/2 J = 4
54.08 (0.01)	-	-	52 {8}	-	-	0.33 (0.02) [0.03]	-	-	179 I = 9/2 J = 4
69.089 (0.002)	69.03	-	52 {8}	66	-	10.6 (0.09) [0.1]	11.11	-	179 I = 9/2 J = 4

Energy [eV]			Γ_γ [meV]			Γ_n [meV]			Isotope & Spin
RPI	ENDF B-VI	Moxon[2]	RPI	ENDF B-VI	Moxon[2]	RPI	ENDF B-VI	Moxon[2]	
73.589 (0.002)	73.53	-	52 {8}	66	-	9.2 (0.1) [0.4]	8.889	-	179 I = 9/2 J = 4
76.702 (0.005)	76.63	-	52 {8}	66	-	3.26 (0.06) [0.04]	2.818	-	179 I = 9/2 J = 5
83.013 (0.004)	82.94	-	52 {8}	66	-	4.69 (0.07) [0.06]	6.667	-	179 I = 9/2 J = 4
85.433 (0.003)	85.42	-	52 {8}	66	-	11.8 (0.2) [0.4]	6.364	-	179 I = 9/2 J = 5
92.125 (0.004)	92.07	-	52 {8}	66	-	11.7 (0.2) [0.2]	55.56	-	179 I = 9/2 J = 4
92.7852 (0.003)	-	-	52 {8}	-	-	27 (0.3) [0.6]	-	-	179 I = 9/2 J = 5
101.382 (0.001)	101.2	-	52 {8}	66	-	113.8 (0.7) [1]	118.2	-	179 I = 9/2 J = 5
103.821 (0.006)	103.7	-	52 {8}	66	-	9.8 (0.2) [0.2]	9.091	-	179 I = 9/2 J = 5
107.858 (0.004)	107.8	-	52 {8}	66	-	9.5 (0.1) [0.1]	14.44	-	179 I = 9/2 J = 4
117.278 (0.002)	117.2	-	44 (1) [2]	66	-	31 (0.4) [1]	35.46	-	179 I = 9/2 J = 5
120.165 (0.008)	120.1	-	52 {8}	66	-	3.46 (0.08) [0.03]	2.444	-	179 I = 9/2 J = 4
121.86 (0.03)	121.9	-	52 {8}	66	-	3.7 (0.3) [0.07]	32.22	-	179 I = 9/2 J = 4
122.689 (0.005)	122.6	-	52 {8}	66	-	15.8 (0.4) [0.4]	23.64	-	179 I = 9/2 J = 5
130.024 (0.005)	129.9	-	52 {8}	66	-	10.2 (0.2) [0.09]	11.11	-	179 I = 9/2 J = 4
137.426 (0.004)	137.2	-	52 {8}	66	-	36.6 (0.7) [0.7]	45.46	-	179 I = 9/2 J = 5

Energy [eV]			Γ_γ [meV]			Γ_n [meV]			Isotope & Spin
RPI	ENDF B-VI	Moxon[2]	RPI	ENDF B-VI	Moxon[2]	RPI	ENDF B-VI	Moxon[2]	
144.341 (0.006)	144.2	-	52 {8}	66	-	32 (0.9) [2]	25.46	-	179 I = 9/2 J = 5
147.103 (0.006)	147	-	52 {8}	66	-	12.2 (0.3) [0.05]	12.22	-	179 I = 9/2 J = 4
156.393 (0.003)	156.3	-	58 (2) [2]	66	-	45 (0.7) [1]	40	-	179 I = 9/2 J = 5
158.835 (0.008)	-	-	52 {8}	-	-	4.7 (0.1) [0.009]	-	-	179 I = 9/2 J = 4
165.807 (0.005)	165.7	-	52 {8}	66	-	23.7 (0.4) [0.6]	20	-	179 I = 9/2 J = 5
174.904 (0.008)	174.9	-	52 {8}	66	-	77 (2) [9]	144.4	-	179 I = 9/2 J = 4
177.996 (0.006)	177.9	-	52 {8}	66	-	66 (2) [6]	25.46	-	179 I = 9/2 J = 5
182.790 (0.005)	182.6	-	52 {8}	66	-	32.8 (0.6) [0.5]	53.33	-	179 I = 9/2 J = 4
188.75 (0.02)	-	-	52 {8}	-	-	6.1 (0.4) [0.4]	-	-	179 I = 9/2 J = 4
189.953 (0.007)	188.5	-	52 {8}	66	-	20.2 (0.4) [0.5]	29.09	-	179 I = 9/2 J = 5
191.25 (0.06)	192.9	-	52 {8}	66	-	0.91 (0.08) [0.05]	5.556	-	179 I = 9/2 J = 4
198.052 (0.008)	197.9	-	52 {8}	66	-	16.1 (0.3) [0.2]	18.18	-	179 I = 9/2 J = 5
^{180}Hf									
72.4640 (0.0007)	72.6	-	28.9* (0.2)	46	-	63.3* (0.2)	54	-	180 I = 0 J = ½
172.062 (0.003)	171.7	-	52 (0.4) [2]	78	-	115 (0.8) [2]	116	-	180 I = 0 J = ½

* These resonances were fitted using a narrow energy range and manually changing values. They were then not allowed to vary during the fit over the full energy range as the values would run away due to the number of overlapping resonances. Therefore the error due to resolution function uncertainties was not able to be determined.

** Only one resonance in ^{178}Hf was found to be sensitive to $\Gamma\gamma$, therefore this value was applied to the other two resonances.

The resonance parameters determined for the ^{176}Hf and ^{178}Hf resonances near 8 eV are significantly different than the few previous measurements available. The biggest change is in the Γ_n value in the ^{176}Hf resonance at 7.8891 eV. The value quoted by Moxon of 4.71 meV is approximately one third the value determined in this analysis of 10.15 meV. The value quoted by Moxon, which is also the ENDF/B-VI value, is quoted with an extremely high error (over 100%) and it is therefore not surprising to see a large change in this parameter. The Γ_n determined from this analysis for this resonance seems to provide a much more reliable value than was previously available. As recommended by Moxon, this analysis has lead to the same conclusion that a more highly enriched ^{176}Hf sample would allow a more accurate set of resonance parameters to be determined for this resonance.

The thermal cross sections based on the fitted RPI parameters and the ENDF/B-VI parameters are shown in Table IX. As expected, the RPI value with its error is consistent with the ENDF/B-VI value. This is due to good agreement between the ENDF/B-VI and fitted RPI resonance parameters at low energies. The majority of previous hafnium measurements were done in the thermal energy region, making the lower energy hafnium resonance parameters quite reliable, with the exception of the two resonances at 8 eV.

Table IX: Hafnium thermal cross section based on ENDF/B-VI and RPI resonance parameters

Thermal Cross Section (σ_t at 0.0253 ev)	
ENDF/B-VI	114.5 barns
RPI	115.3 ± 0.8 barns

Resonance integrals for each of the hafnium isotopes analyzed were calculated along with errors. The resonance integrals were calculated based on the resonance parameters determined in this analysis (shown in Table VIII). ENDF/B-VI resonance parameters were used outside the energy range analyzed in this work for the resonance integral calculations. NJOY[14] and INTER[15] were used to calculate the resonance integral for the hafnium isotopes. Table X shows the calculated resonance integral for each of the hafnium isotopes analyzed compared to those based on other evaluated hafnium resonance parameters. As shown in Table X, significant changes in some of the hafnium isotopic resonance integrals were calculated based on the resonance parameters determined in this analysis. The elemental hafnium resonance integral calculated from the abundance weighted sum of the isotopic resonance integrals also differs from

resonance integrals calculated from other data sets. Table XI shows the resonance integrals calculated from ENDF/B-VI and RPI resonance parameters with an integration region from 0.5 -200 eV. These were calculated to show the energy region that only includes resonances that were analyzed in this work. The errors shown in Tables X and XI for the RPI values are based on the error estimates presented in Table VIII and represent one standard deviation[3].

Table X: Resonance integrals calculated from resonance parameters determined in this analysis (labeled RPI) compared with those from other evaluated hafnium resonance parameters; all were integrated from 0.5 – 1.0 x 10^5 eV.

[Values in barns]	**Hf 174**	**Hf 176**	**Hf 177**	**Hf 178**	**Hf 179**	**Hf 180**	**Natural**
JEF-2.2	320.3	612.8	7232	1922	543.1	35.44	1983
JENDL-3.2	361.8	892.7	7209	1914	521.6	33.85	1987
ENDF/B-VI	355.1	400.2	7221	1915	548.6	34.28	1968
RPI	375 ± 20	692 ± 2	7196 ± 8	1872 ± 4	506 ± 3	28.8 ± 0.1	1959 ± 2

Table XI: Resonance integrals calculated from resonance parameters determined in this analysis (labeled RPI) and from ENDF/B-VI parameters, integrated from 0.5 – 200 eV.

[Values in barns]	**Hf 174**	**Hf 176**	**Hf 177**	**Hf 178**	**Hf 179**	**Hf 180**	**Natural**
ENDF/B-VI	324.5	381.6	7158	1902	506.7	30.66	1944.8
RPI	345 ± 20	673 ± 2	7139 ± 8	1859 ± 4	464 ± 3	25.2 ± 0.1	1937 ± 2

6 Conclusions

This paper presents the results of both capture and transmission experiments using various hafnium samples. These experiments provided energy dependent transmission and yield data that were analyzed using the R-matrix Bayesian fitting code SAMMY. The transmission experiments were done utilizing a ^{6}Li glass scintillation detector at a ~15 m flight path for low energy measurements (0.005-10 eV), and a similar detector at ~25 m for higher energy measurements (10-200 eV). A sixteen section NaI(Tl) multiplicity detector was used for the capture experiments at a flight path of ~25 m.

The samples used in these experiments were various thicknesses of metallic hafnium and deuterated nitric acid solutions of isotope-enriched hafnium. The isotope-enriched samples were designed to provide experimental data that could be used to determine resonance parameters for the overlapping resonances of ^{176}Hf and ^{178}Hf at ~8 eV. The liquid solution samples were needed to provide sufficiently thin samples to prevent saturation or blacking out of the 8 eV resonance pair in capture and transmission experiments. The only previously found ^{176}Hf parameters for the 8 eV resonance were from measurements done by Moxon et al.[2], which have an extremely high quoted error and are referred to as “not well known” in the report. This analysis provides a much more accurate set of resonance parameters for this 8 eV doublet. A combined analysis of capture and transmission data using SAMMY was performed to determine resonance parameters for all stable isotopes of hafnium in the energy range of 0.005-200 eV.

Resonance integrals for each hafnium isotope, based on the fitted resonance parameters, were calculated using the NJOY and INTER codes. The ^{176}Hf resonance integral, based on this work, is approximately 73% higher than that using ENDF/B-VI parameters. This change is primarily due to the significant change in ^{176}Hf resonance parameters near 8eV. This change is not surprising, given the small amount of experimental data available for the overlapping ^{176}Hf and ^{178}Hf resonances at this energy and the high level of uncertainty in previous work. A much smaller change to the ^{178}Hf resonance integral, which is approximately 2% lower than ENDF/B-VI and in the opposite direction of the ^{176}Hf resonance integral change, is also primarily due to the changes in the ^{178}Hf resonance parameters near 8eV. This change in the ^{178}Hf resonance integral is lower in magnitude because the 8eV resonance is a much smaller contributor to the resonance integral for ^{178}Hf.

The hafnium experimental data and resonance parameters provided are a significant improvement over previous measurements due to improved sample design, experimental resolution and analysis tools.

7 References

[1] H. I. Liou, J. Rainwater, G. Hacken, and U. N. Singh, *Phys. Rev. C,* 11, 2022 (1975).

[2] M. C. Moxon, D. A. J. Endacott, T. J. Haste, J. E. Jolly, J. E. Lynn and M. G. Sowerby, "Differential Neutron Cross-Sections of Natural Hafnium and Its Isotopes for Neutron Energies Up to 30 eV", *United Kingdom Atomic Energy Authority*, AERE – R 7684 (1974)

[3] M. Trbovich, "Hafnium Cross Sections And Resonance Analysis", Ph.D. Thesis, Rensselaer Polytechnic Institute (2003)

[4] RC Block, Y. Danon, R.E. Slovacek, C.J. Werner, G. Youk, J.A. Burke, N.J. Drindak, F. Feiner, J.A. Helm, J.C. Sayres and K.W. Seeman, Neutron Time-of-Flight Measurements at the Rensselaer LINAC, Proc. of Int'l. Conf. on Nuclear Data for Sci. & Technol., Gatlinburg, Tenesseee, May 9-13, 1994, pp 81-85.

[5] Y. Danon, "Design and Construction of the RPI Enhanced Thermal Neutron Target and Thermal Cross Section Measurements of Rare Earth Isotopes," Ph.D. Thesis, Rensselaer Polytechnic Institute (1993).

[6] B. E. Moretti, "Molybdenum Neutron Transmission Measurements and the Development of An Enhanced Resolution Neutron Target," Ph.D. Thesis, Rensselaer Polytechnic Institute (1996).

[7] M. E. Overberg, "Development of an Improved Epithermal Neutron Target and Measurement of the Resolution Function to 350 eV," MS Thesis, Rensselaer Polytechnic Institute (1997).

[8] N. J. Drindak, "A Multiplicity Detector for Neutron Capture Measurements," Masters Thesis, Rensselaer Polytechnic Institute (1987).

[9] N. M. Larson, "Updated Users Guide for SAMMY: Multilevel R-Matrix fits to Neutron Data Using Bayes' Equations," ORNL/TM-9179/R5, Lockheed Martin Energy Research Corporations, Oak Ridge National Laboratory (2000).

[10] D. P. Barry, "Neodymium Neutron Transmission and Capture Measurements and the Design of an Improved Resolution Transmission Detector", Ph.D. Thesis, Rensselaer Polytechnic Institute (2003)

[11] D. P. Barry, M. J. Trbovich, Y. Danon, R. C. Block, R. E. Slovacek, G. Leinweber, J. A. Burke, N. J. Drindak, "Neutron Transmission and Capture Measurements and Resonance Parameter Analysis of Neodymium From 1.0 eV To 500 eV". *Nuclear Science and Engineering*: 153, 8-2, (2006).

[12] Private communication with M. Lubert, Rensselaer Polytechnic Institute

[13] S. F. MUGHABGHAB, M. DIVADEENAM and N. E. HOLDEN, *Neutron Cross Sections*, Academic Press, New York and London (1984).

[14] R. E. MacFarlane and D. W. Muir, "The NJOY Nuclear Data Processing System Version 91," LA-12740-M, Los Alamos National Laboratory (Oct. 1994).

[15] C. L. Dunford, Informal report, “ENDF Utility Codes Release 6.12” (April 2001).